

Organic/Inorganic Hybrid Composites from Cubic Silsesquioxanes

Jiwon Choi,[†] Jason Harcup,[‡] Albert F. Yee,[§] Quan Zhu,[‡] and Richard M. Laine^{*,†,‡}

Contribution from the Departments of Materials Science and Engineering, Chemistry, Macromolecular Science and Engineering Center, H.H Dow Building, University of Michigan, Ann Arbor, Michigan 48109-2136, and Institute of Materials Research & Engineering, 3 Research Link, Singapore 117602

Received March 19, 2001

Abstract: A new class of epoxy nanocomposites with completely defined organic/inorganic phases was prepared by reacting octakis(glycidyl dimethylsiloxy)octasilsesquioxane [(glydicylMe₂SiOSiO_{1.5})₈] (OG) with diamino-diphenylmethane (DDM) at various compositional ratios. The effects of reaction curing conditions on nanostructural organization and mechanical properties were explored. A commercial epoxy resin based on the diglycidyl ether of bisphenol A (DGEBA) was used as a reference material throughout these studies. FTIR was used to follow the curing process and to demonstrate that the silsesquioxane structure is preserved during processing. OG/DDM composites possess comparable tensile moduli (E) and fracture toughness (K_{IC}) to, and better thermal stabilities than, DGEBA/DDM cured under similar conditions. Dynamic mechanical analysis and model reaction studies suggest that the maximum cross-link density is obtained at $N = 0.5$ (NH₂:epoxy groups = 0.5) whereas the mechanical properties are maximized at $N = 1.0$. Digestion of the inorganic core with HF followed by GPC analysis of the resulting organic tether fragments when combined with the model reaction studies confirms that, at $N = 0.5$, each organic tether connects four cubes, while, at $N = 1.0$, linear tethers connecting two cubes dominate the network structure. Thus, well-defined nanocomposites with controlled variation of the organic tether architecture can be made and their properties assessed.

Introduction

Although polymers offer good processibility and relatively low cost compared to metals or ceramics, pure polymeric materials often face applications limitations because their inherent properties are poor, e.g., low modulus and/or low thermal stability. Many types of polymer–filler macroscopic composites have been developed to overcome these drawbacks. Usually, the properties of these composites can be estimated using the rule of mixtures.^{1,2} However, this method fails when interfacial interactions between components begin to affect the global properties.^{1,2} These interactions become more pronounced as the sizes of the individual component phases decrease.^{3–6} In principle, as the length scales of the component phases approach the range of a few nanometers, the expected global properties will be most strongly affected by interfacial interactions rather than bulk phase properties. For example, polyamide-6 filled with

even small amounts of exfoliated clay^{7,8} exhibits significant improvements in tensile modulus that can only be explained by extensive organic/inorganic interfacial interactions.

Because nanocomposite materials, wherein interfacial interactions dominate global properties, can offer properties not anticipated (nonlinearly related) by (to) knowledge of bulk phase properties; the potential exists to make materials with quite novel properties. To best understand what this potential is, access to very well defined nanocomposites must be developed. Of equal importance is access to nanocomposite materials wherein the nanoarchitecture can be extensively and selectively varied such that one can probe the effects of changes in nanoarchitecture on global properties.

In a recent series of papers,^{9–16} we described synthetic routes to nanocomposite materials and/or precursors based on cubic silsesquioxanes (or polyhedral oligomeric silsesquioxanes, POSS) macromonomers. In these materials (Scheme 1), the cubic silica core is rigid and completely defined (0.53 nm diameter) and eight organic functional groups (R) are appended to the vertexes of the cube via O–SiMe₂– (spacer) linkages. These materials provide access to nanocomposites wherein the

* Corresponding author. Telephone: 734-763-4970/4-6203. Fax: 734-763-4788. E-mail: talsdad@umich.edu.

[†] Macromolecular Science and Engineering Center, University of Michigan.

[‡] Departments of Materials Science and Engineering, Chemistry, University of Michigan.

[§] Institute of Materials Research & Engineering, Singapore.

(1) Matthews, F. L.; Rawlings, R. D. *Composites Materials: Engineering and Science*; Chapman & Hall: London, U.K., 1994; p 14.

(2) Jackson, G. V.; Orton, M. L. In *Particulate-filled Polymer Composites*; Rothon, R., Ed.; Longman scientific & technical: Essex, U.K., 1995; p 317.

(3) Verghese, N. E.; Lesko, J. J. In *Reinforced Plastics Durability*; Pritchard, G., Ed.; Woodhead publishing Ltd: Cambridge, U.K., 1999; p 336.

(4) Demjen, Z.; Pukanszky, B.; Nagy, J. *Composites, Part A* **1998**, *29*, 323.

(5) Chiu, H.; Wang, J. J. *Appl. Polym. Sci.* **1998**, *68*, 1387.

(6) Li, T.; Zhang, M.; Zhang, K.; Zeng, H. *Comput. Sci. Technol.* **2000**, *60*, 465.

(7) Kojima, Y.; Usuki, A.; Kawasumi, M. *J. Mater. Res.* **1993**, *8*, 1185.

(8) Kojima, Y.; Usuki, A.; Kawasumi, M.; Okada, A.; Kurauchi, T.; Kamigaito, O. *Mater. Life* **1993**, *5*, 13.

(9) Sellinger, A.; Laine, R. M. *Macromolecules* **1996**, *29*, 2327.

(10) Zhang, C.; Laine, R. M. *J. Organomet. Chem.* **1996**, *521*, 199.

(11) Sellinger, A.; Laine, R. M. *Chem. Mater.* **1996**, *9*, 1592.

(12) Laine, R. M.; Zhang, C.; Sellinger, A.; Viculis, L. *Appl. Organomet. Chem.* **1998**, *12*, 715.

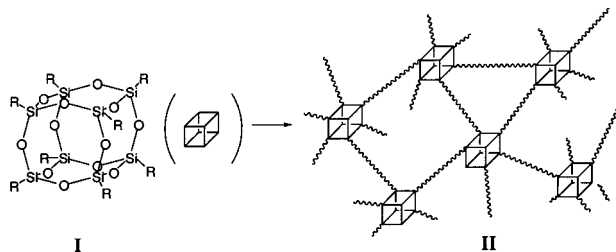
(13) Gravel, M. C.; Zhang, C.; Dinderman, M.; Laine, R. M. *Appl. Organomet. Chem.* **1999**, *13*, 329.

(14) Zhang, C.; Babonneau, F.; Bonhomme, C.; Laine, R. M.; Soles, C. L.; Hristov, H. A.; Yee, A. F. *J. Am. Chem. Soc.* **1998**, *120*, 8380.

(15) Zhang, C.; Laine, R. M. *J. Am. Chem. Soc.* **2000**, *122*, 6979.

(16) Laine, R. M.; Choi, J.; Lee, I. *Adv. Mater.* **2001**, *13*, 800.

Scheme 1. Formation of Nanocomposites with Defined, Discontinuous Organic/Inorganic Phases (II) from Cubic Silsesquioxanes (I) via Cross-Linkable Functional Groups R



architecture of the organic components between the cubes can be varied in a systematic manner. In principle, the reactions that form organic tethers *between* cubes will also be well defined so as to ensure complete control of the length scales of each component in the resulting nanocomposite. To this end, we have developed routes to thermoplastic and thermoset methacrylate nanocomposites, as well as epoxy resin, hydrocarbon-linked, amide, and imide-linked nanocomposites.^{9–16} In these materials, the organic tether lengths are anticipated to be of the order of 3–5 nm and well within the dimensions normally ascribed to “interphase” materials (see below) that form in macroscopic composites.

With synthetic methodologies in place, it is now possible to initiate studies designed to demonstrate whether nanocomposite materials based on silsesquioxanes will exhibit global properties that are not simply the sum of the components.^{9–26} A further goal is to develop a detailed understanding of nanoarchitecture design-precursor synthesis-processing-mechanical properties relationships to (1) establish a comprehensive picture of nanocomposite behavior, (2) identify design and synthesis parameters to optimize properties, and (3) develop methods of predicting and tailoring such behavior.

Our first objective is to prove that the processed composites are indeed nano and that the chemistry involved in creating them does in fact lead to well-defined interactions between the organic components and the cube. A second objective is to establish standard test and analytical procedures for these materials. A third objective is to explore the use of modeling as a means of predicting/understanding global mechanical properties as a function of organic tether (links between cubes) structure, flexibility, and mobility.¹⁶

In early work,¹⁴ we demonstrated that certain hydrocarbon-linked cube nanocomposites form well-ordered materials that exhibited a high degree of microporosity wherein pore sizes and size distributions are controlled by tether length and defects (missing cubes). We begin here a series of papers on epoxy

resin nanocomposite systems including synthesis, processing, and mechanical properties evaluation. These efforts were initiated because the literature on the design, processing, and mechanical properties of epoxy resins provides an extensive base of information for comparison. Thus, epoxy nanocomposites should allow us to thoroughly test the concepts suggested to be inherent in the use of nanodesigned materials. Some background discussion on epoxy materials follows.

Epoxy resins are among the most commercially successful materials known especially as composite matrices but also as coating materials and adhesives.^{27–32} Many kinds of epoxy-amine systems have been studied to examine the effects of variables such as prepolymer molecular weight, formulation stoichiometry, and composite microstructure on global properties.^{33–46} Among them, resins based on the diglycidyl ether of bisphenol A (DGEBA) are particularly well studied because the molecular weight of DGEBA can be adjusted via condensation reactions and properties such as viscosity can be optimized for particular applications. Likewise, diaminodiphenyl methane (DDM) is a commonly used curing agent.^{33–35,47} This study uses DGEBA and DDM as a standard resin. For the same reason, we have chosen the glycidyl unit on the “spacer” cube core for our first set of comparative tests and DDM as our standard curing agent. Scheme 2 suggests the expected outcome of reacting the octaglycidyl spacer cube with DDM at the commonly used resin stoichiometry of $N = 0.5$ ($N = \text{no. of amine groups in DDM}/\text{No. of epoxides groups in OG}$). In this scheme, a complete reaction of DDM with 4 different cubes demonstrates one possible tether structure.

In the resin systems developed here, our goal is to completely decouple the organic and inorganic phases to ensure that we can probe changes in the organic tether architecture alone. We describe such nanocomposites as being completely discontinuous.^{16,48} That is, there are no inorganic bonds between the cubes (inorganic phase) and there are no (very few) organic bonds between the organic tethers as would be present in a wholly

(17) Provatas, A.; Matison, J. G. *Trends Polym. Sci.* **1997**, *5*, 327.

(18) Baney, R. H.; Itoh, M.; Sakakibara, A.; Suzuki, T. *Chem. Rev.* **1995**, *95*, 1409.

(19) Provatas, A.; Luft, M.; Mu, J. C.; White, A. H.; Matison, J. G.; Skelton, B. W. *J. Organomet. Chem.* **1998**, *565*, 159.

(20) Luke, S.; Stoppek-Langer, K. *Appl. Surface. Sci.* **1999**, 144–145, 713.

(21) Mather, P. T.; Jeon, H. G.; Romo-Urbe, A. *Macromolecules* **1999**, *32*, 1194.

(22) Romo-Urbe, A.; Mather, P. T.; Haddad, T. S.; Lichtenhan, J. D. *J. Polym. Sci. Polym. Phys.* **1998**, *36*, 1857.

(23) Tsuchida, A.; Bolln, C.; Sernetz, F. G.; Frey, H.; Mulhaupt, R. *Macromolecules* **1997**, *30*, 7302.

(24) Haddad, T. S.; Lichtenhan, J. D. *Macromolecules* **1996**, *29*, 7302.

(25) For an all organic nanocomposite, see Hillmyer, M. A.; Lipic, P. M.; Hajduk, D. A.; Almdal, K.; Bates, F. S. *J. Am. Chem. Soc.* **1997**, *119*, 2749.

(26) Lipic, P. M.; Hillmyer, M. A.; Bates, F. S. *J. Am. Chem. Soc.* **1998**, *120*, 8963.

(27) Tanaka, Y. In *Epoxy Resins, Chemistry and Technology*; May, C. A., Ed.; Marcel Dekker: New York, 1988; p 9.

(28) Delmonte, J.; Hoggatt, J. T.; May, C. A. In *Epoxy Resins, Chemistry and Technology*; May, C. A., Ed.; Marcel Dekker: New York, 1988; p 885.

(29) Lewis, A. F. In *Epoxy Resins, Chemistry and Technology*; May, C. A., Ed.; Marcel Dekker: New York, 1988; p 653.

(30) Tess, R. W. In *Epoxy Resins, Chemistry and Technology*; May, C. A., Ed.; Marcel Dekker: New York, 1988; p 719.

(31) Goodman, S. H. In *Handbook of Thermoset Plastics*; Goodman, S. H., Ed.; Noyes Publ.: Westwood, NJ, 1998; p 193.

(32) Smith, G.; May, C. A. In *Epoxy Resins*; Gould, R. F., Ed.; American Chemical Society: Washington, DC, 1970; p 140.

(33) Cardwell, B. J.; Yee, A. F. *J. Mater. Sci.* **1998**, *33*, 5473.

(34) Kimoto, M.; Mizutani, K. *J. Mater. Sci.* **1997**, *32*, 2479.

(35) Engelberg, P. I.; Tesoro, G. C. *Polym. Eng. Sci.* **1990**, *30*, 303.

(36) Palmese, G. R.; McCullough, R. L. *J. Appl. Polym. Sci.* **1992**, *46*, 1863.

(37) Vanlandingham, M. R.; Eduljee, R. F.; Gillespie, L. W., Jr. *J. Appl. Polym. Sci.* **1999**, *71*, 699.

(38) Skoulis, T. P.; Mccullough, R. L. *J. Appl. Polym. Sci.* **1996**, *62*, 481.

(39) Levita, G.; De Petris, S.; Marchetti, A.; Lazzeri, A. *J. Mater. Sci.* **1991**, *26*, 2348.

(40) Butta, E.; Levita, G.; Marchetti, A.; Lazzeri, A. *Polym. Eng. Sci.* **1986**, *26*, 63.

(41) Truong, V. T. *Polymer* **1990**, *31*, 1669.

(42) Urbaczewski-Espuche, E.; Galy, J.; Gerard, J.; Pascault, J.; Sauteau, H. *Polym. Eng. Sci.* **1991**, *31*, 1572.

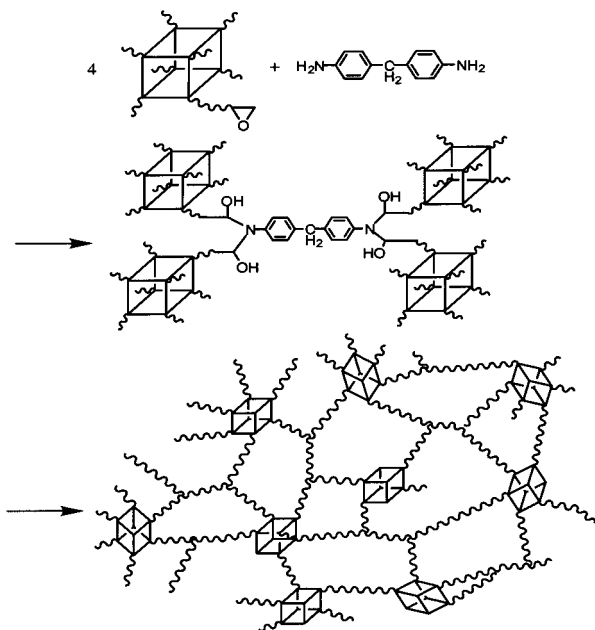
(43) Crawford, E. D.; Lesser, A. J. *Polym. Eng. Sci.* **1999**, *39*, 385.

(44) Denq, B.; Hu, Y.; Chen, L.; Chiu, W.; Wu, T. *J. Appl. Polym. Sci.* **1999**, *74*, 229.

(45) Gupta, V. B.; Dzal, L. T.; Lee, C. Y.-C. *Polym. Eng. Sci.* **1985**, *25*, 812.

(46) Morgan, R. J.; Kong, F.; Walkup, C. M. *Polymer* **1984**, *25*, 375.

(47) Tanaka, Y.; Bauer, R. S. In *Epoxy Resins, Chemistry and Technology*; May, C. A., Ed.; Marcel Dekker: New York, 1988; p 465.

Scheme 2. Formation of Nanocomposites from Epoxy-Functionalized Cubic Silsesquioxanes^a

^a The ratio of amine groups (NH₂) to epoxide groups is 1:2. Organic tethers can link up to 4 cubes.

organic resin. This situation will not only allow us to probe organic tether structural effects on global properties, it should also allow us to develop an understanding of the behavior of interphase materials in macroscopic organic/inorganic composites.^{49–52}

In macroscopic composites the interfacial interactions between components are known to create a buffer region, often called the “interphase”, between the components. The interphase is thought to have properties that are nonlinearly related to the properties of the bulk components.^{49–52} This interphase region is thought to have dimensions of the order of 2–4 nm. In our nanocomposites, all organic and inorganic components are discontinuous at 1–4 nm length scales; hence, the resulting materials might be considered to be completely interphase if the cubes and the organic tethers are considered to be separate phases. This designation should be considered to be notional because thermodynamically there is only one phase. These materials then provide a rare opportunity to understand how such materials can affect macroscopic composite properties.

Experimental Section

Materials. Tetramethylammonium hydroxide (25 wt % in MeOH), tetraethoxysilane, dimethylchlorosilane, allyl glycidyl ether, dicyclopentadiene, hydrated chloroplatinic acid, glacial acetic acid, and triphenylphosphine were purchased from Aldrich (Milwaukee, WI) and used without further purification. 4,4'-Diaminodiphenylmethane (DDM) was purchased from Alfa Aesar (Ward Hill, MA). The diglycidyl ether

(48) Laine, R. M.; Asuncion, M.; Baliat, S.; Dias Filho, N. L.; Harcup, J.; Sutorik, A. C.; Viculis, L.; Yee, A. F.; Zhang, C.; Zhu, Q. In *Organic/Inorganic Hybrid Materials II, MRS Symp. Ser., Vol. 576*; Klein, L., De Guire, M., Lorraine, F., Mark, J., Eds.; Mater. Res. Soc.: Warrendale, PA, 1999; p 3.

(49) Delong, J.; Hook, K. J.; Rich, M. F.; Drzal, L. T. In *Composites Materials*; Ishida, H., Ed.; Elsevier Press: New York, 1990; p 87.

(50) Large-Toumi, B.; Salvia, M.; Vincent, L. In *Fiber, Matrix and Interface Properties*; ASTM STP 1290; Spragg, C. J., Drzal, L. T., Eds.; ASTM: West Conshohocken, PA, 1996; p 182.

(51) Li, T.; Zhang, M.; Zhang, K.; Zeng, H. *Comput. Sci. Technol.* **2000**, *60*, 465.

(52) Mäder, E.; Jacobasch, H.-J.; Grundke, K.; Gietzelt, T. *Composites, Part A* **1996**, *27*, 907.

Table 1. GPC Data for Spacer Cube and OG

	calcd ^a	M _n	M _w	PDI ^b
spacer cube	1017	992	1005	1.01
OG	1931	1514	1546	1.02

^a Theoretical molecular weight. ^b Polydispersity index.

of bisphenol A (DGEBA) (DER 331, MW 372) was obtained from Dow Chemicals (Midland, MI).

Syntheses. Catalyst. Platinum dicyclopentadiene [Pt(dcp)] was synthesized by following a literature method.⁵³ Hydrated chloroplatinic acid, 500 mg (3.78 mmol), was dissolved in glacial acetic acid (1.1 mL) in a 25 mL flask and then diluted with 2.0 mL of water. The mixture was heated to 70 °C and 0.4 mL of dicyclopentadiene added. The solution was stirred vigorously for 24 h at temperature and cooled. The solid product was filtered off, decolorized with charcoal, and recrystallized using THF to give 190 mg (yield 51%).

Octakis(dimethylsiloxypolyglycidyl ether)silsesquioxane (OG). The synthesis of OG followed published procedures.¹¹ Octaanion solution [Me₄N⁺]₈[SiO_{2.5}]₈ was prepared by mixing tetramethylammonium hydroxide, methanol, and deionized water followed by dropwise addition of tetraethoxysilane under nitrogen. Octahydrido spacer cube, [HMe₂SiO_{1.5}]₈, was made by reaction of the octaanion with dimethylchlorosilane. Finally, OG was prepared via catalyzed hydrosilylation of allyl glycidyl ether with octahydrido spacer cube using Pt(dcp). Product purity was confirmed by ¹H NMR.¹¹ Molecular weights and distributions were measured by GPC as shown in Table 1. Because the hydrodynamic volume of “spherical” spacer cube and OG are smaller than the linear polystyrenes used for GPC calibration, the measured molecular weights appear smaller than the theoretical values. Furthermore, the nonlinear change in molecular weights of cubes with respect to those of polystyrenes resulted in a larger discrepancy in OG than in spacer cube.

Curing Optimization Tests. Prior to conducting mechanical tests, studies were conducted to determine the point after which no further processing would lead to improvements in mechanical properties. To this end, using the general procedures described in the following section, both DGEBA/DDM and OG/DDM materials were cured at temperatures ranging from 100 to 200 °C for periods of 3–20 h. It was determined that for OG/DDM (and DGEBA/DDM), curing for 6 h at 150 °C was sufficient for reproducible modulus and fracture toughness. However, in conjunction with work with other epoxy cubic silsesquioxanes,¹⁶ curing for 10 h was adopted for a comprehensive study, to be published at a later date.⁵⁴

Mechanical Test Samples. Two different sample sets were prepared. The first set consisted of DGEBA cured with DDM and the second set consisted of OG cured with DDM. In formulating samples, a variable *N* was defined:

$$N = \frac{\text{no. of amine groups in DDM}}{\text{no. of epoxy rings in DGEBA or in OG}}$$

Thus, when *N* = 1, there are equal numbers of NH₂ groups and epoxy rings in the sample mixture. A conventional stoichiometric ratio of 2 mol of amine to 1 mol of epoxy would occur for *N* = 0.5. Table 2 shows the formulations of DGEBA and OG samples with various *N*'s. Conventionally, curing agents in epoxy formulations are measured by Phr (parts of amines per hundred of resins; ratio of amine weights vs epoxy weights) and thus these values are included for comparison. The total mass of the mixture for each sample was kept constant at 12 g.

Materials were weighed into an aluminum pan (61.5 mm diameter × 18 mm) and mixed by hand. The mixture was melted and degassed at 140–150 °C under vacuum for 7–15 min. When the mixture became homogeneous and no more bubbles emerged, it was poured into an aluminum mold previously surface-coated with Teflon mold release agent and preheated to 150 °C. The mixture was then cured at 150 °C

(53) Apfel, M. A.; Finkelmann, H.; Janni, G. M.; Laub, R. J.; Lüthmann, B.-H.; Price, A.; Roberts, W. L.; Shaw, T. J.; Smith, C. A. *Anal. Chem.* **1985**, *57*, 651.

(54) Choi, J.; Lee, I.; Laine, R. M. Manuscript in preparation.

Table 2. Compositions of DGEBA/DDM and OG/DDM Composites

	N for DGEBA				N for OG						
	0.5	0.75	1	1.25	0.3	0.5	0.75	1	1.25	1.5	2
wt % DDM	21.0	28.5	34.7	40.0	10.9	17.0	23.5	29.1	33.9	38.1	45.1
Phr ^a DDM	26.6	40.0	53.2	66.5	12.3	20.5	30.8	41.0	51.2	61.5	82.0

^a Phr: Parts of DDM/hundred DGEBA resin by weight.⁴⁷

under nitrogen for 10 h. After the mold cooled, the sample was removed and kept in a desiccator prior to testing.

Characterization. Gel Permeation Chromatography (GPC). Molecular weights and distributions of octahydrodo spacer cube and OG were measured using a Waters GPC system, equipped with RI and UV detectors, a Styragel column set (7.8 × 300, HR-high resolution 0.5, 1, 3, 4), and a PL-DCU data capture unit. These 4 columns are special units suitable for measuring small molecules including epoxies and amines. The system was calibrated using polystyrene standards. THF was used as the eluent, at a flow rate of 1.0 mL/min. GPC was also used to analyze the tether structures following dissolution of the core (see below).

NMR Analyses. All ¹H NMR analyses were performed with a Varian INOVA 400 spectrometer at 400 MHz with a 6000 Hz spectral width, a relaxation delay of 3.5 s, a pulse width of 38°, and 30k data points. All the spectra were recorded in CDCl₃ medium with CDCl₃ signal as an internal reference at 7.259 ppm.

Fourier Transform Infrared Spectroscopy (FTIR). Diffuse reflectance IR spectra (DRIFTS) were obtained using a Mattson Galaxy Series FTIR 3000 spectrometer (Mattson Instruments, Inc.). Optical grade potassium bromide (KBr, International Crystal Laboratories, Garfield, NJ) was used as a background material. Cured sample (5 mg) and KBr crystal (500 mg) were ground together using an alumina mortar and pestle. The ground powder was packed into a sample holder and leveled off with a glass plate to give a smooth surface. The holder was placed in the sample chamber, and the spectrum was recorded under dry N₂ purge. At least 100 scans were averaged for each spectrum. The resolution was ±4 cm⁻¹.

Thermal Gravimetric Analysis (TGA). Thermal stabilities of materials under nitrogen or air were tested using a 2960 simultaneous DTA-TGA Instrument (TA Instruments, Inc., New Castle, DE). Samples (15–25 mg) were loaded in platinum pans and ramped to 1000 °C (5 °C/min/N₂). The N₂ or air flow rate was 60 mL/min.

Differential Scanning Calorimetry (DSC). Calorimetry was performed on materials using a Perkin-Elmer DSC-7 (Perkin-Elmer Co., Norwalk, CT). The N₂ flow rate was 60 mL/min. Sample (10–15 mg) was placed in a pan and ramped to 600 °C (5 °C/min/N₂) without capping. The heat flow difference between the reference blank and the sample pan was recorded.

Dynamic Mechanical Analysis (DMA). Dynamic mechanical behavior of cured samples was studied using a TA instruments 2980 dynamic mechanical analyzer (New Castle, DE). Cured samples were polished to ≈3.0 × 13.0 × 30.0 mm and mounted on a single cantilever clamp. The mechanical properties were measured under nitrogen in step mode every 10 °C from -50 to 200 °C. Prior to each measurement, the environment was kept at the setting temperature for 10 min to ensure thermal equilibration.

Tensile Modulus and Fracture Toughness. Fresh samples removed from the aluminum mold had rough edges due to overflow. These edges were polished using a polish wheel with 180-, 600-, and 1200-grit SiC paper. After polishing, average dimensions were 3.0 × 13.0 × 170.0 mm (errors < ±0.2 for width and thickness and < ±0.5 for length).

A screw driven Instron 4502 was used to measure elastic moduli (*E*) and the critical stress intensity factors (*K*_{IC}). Sample dimensions were average values of three points for each sample. The elastic moduli were obtained following ASTM standard [No. E111 (1997)] except that the sample geometry was a rectangular bar instead of a dog bone. The ratio of the longitudinal length to the width under tension after clamping was always kept ≥8 to ensure that ratio of the portion under uniaxial tension was >4. The cross-head speed was set at 1 mm/min. Data were recorded at a speed of 5 points/s. The tests were stopped at

loads of 200–250 N. Moduli were measured in the initial elastic deformation region.

The critical stress intensity factor (*K*_{IC}) was measured following ASTM standard [No. E399 (1990)] in a tensile mode. A 1 mm notch was made on the sample using a hacksaw and a natural crack was introduced using a new razor blade. The ratio of the crack to the width was 0.35–0.55. The sample was then loaded in the Instron and tested until it broke. The load at fracture was recorded. The critical stress intensity factor was determined from the following equations:

$$K_{IC} = Y\sigma_0 a^{1/2}$$

$$Y = 1.99 - 0.41\left(\frac{a}{w}\right) + 18.70\left(\frac{a}{w}\right)^2 - 38.48\left(\frac{a}{w}\right)^3 + 53.85\left(\frac{a}{w}\right)^4$$

$$\sigma_0 = \frac{P_b}{Bw}$$

Here *P*_b is the load at the fracture, *B* is the sample thickness, *w* is the sample width, and *a* is the crack length.

Tether Structure Investigation. Model Curing Studies. The curing behavior of the epoxy/amine mixtures without the core silsesquioxane was identified using pure allyl glycidyl ether/DDM. The same variable *N* as in OG/DDM composite formulations was used. Allyl glycidyl ether (1 g, 5 mmol) and varying amounts of DDM were kept at 150 °C under N₂ for 10 h. Products were viscous liquids and readily soluble in common solvents, e.g., acetone and chloroform. The disappearance of epoxy rings in the ally glycidyl ether/DDM mixture during reaction curing was monitored by ¹H NMR. Typical epoxide ring ¹H signals at δ 3.14, 2.79, and 2.59 were monitored in CDCl₃ solution. These model materials are also used as standards in the tether structure studies below.

Direct Analysis of Organic Tether Structure by GPC. Nanocomposite organic tethers were isolated by dissolving the silica core with HF and extracting the organic components for GPC analysis. Reference GPC chromatograms were generated using the model compounds prepared above. These products contain ideal tethers without inorganic components (spacer groups), and GPC data can be used to identify peaks in the HF derived tether GPC chromatograms.

Various OG/DDM composites were ground into powders, and 50 mg of each powder was suspended in 3 mL of THF in a polyethylene bottle. A 50 μL portion of 50% HF was added to the solution, and the mixture was kept at room temperature for 2 days. THF and HF were removed with vacuum-drying. The residual material was mixed with freshly dried THF to extract the organic components. Because OG/DDM was very ductile, grinding provided a mixture of fine and coarse powder. The coarsest powders required more than 2 days of digestion and had to be removed by filtration before GPC analysis. In several studies,⁵⁵ we find that HF has no effect on the stability of the tether fragments released during digestion. In GPC analysis, signals were recorded using a UV detector. The elution times for all peaks were compared with reference GPC peaks and properly assigned.

Results and Discussion

Given all of the considerations discussed above, in the following we begin with a detailed analysis of the materials themselves and then the resulting nanocomposites. Thus, the functionalized cube macromonomers and nanocomposites are first characterized separately by FTIR, TGA, and DSC. Then,

(55) Coats, R. O. R.; Tamaki, R.; Vasconcelos, W. L.; Laine, R. M.; *Macromolecules* **2001**, *34*, 5398–5407.

Scheme 3. OG Synthesis Steps

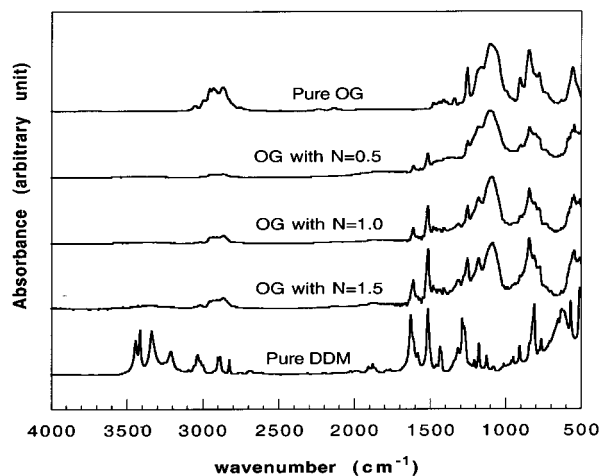
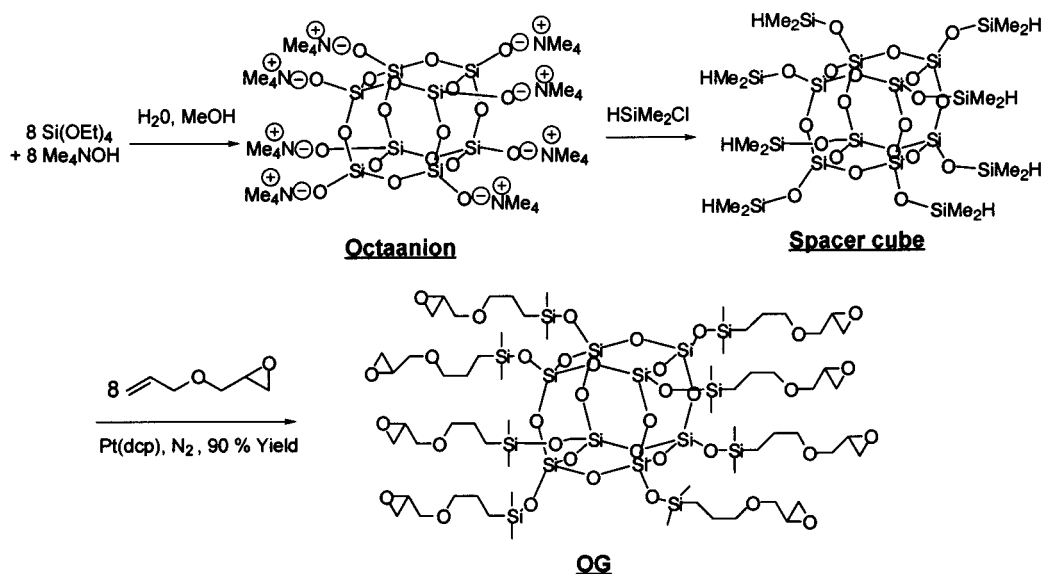


Figure 1. FTIR (DRIFTS) spectra of various OG nanocomposites.

the nanocomposite mechanical properties are evaluated using DMA and tensile/fracture tests. Finally, curing behavior and the network structures of the composites are discussed using model curing studies and direct analysis of the tether architecture by ^1H NMR and GPC.

Synthesis and full characterization of the pure macromonomer are documented elsewhere.²⁸ The general synthetic reactions used are presented in Scheme 3.

DRIFTS. Diffuse reflectance FTIR was used to follow the curing of various formulations and to confirm the preservation of the cube structure in the formed nanocomposites. Figure 1 shows the spectra for several OG nanocomposites with varying values of N . The spectra for pure OG and DDM are included for comparison. The characteristic IR absorption behavior of epoxies and siloxanes are summarized in Table 3. A sharp, strong, and symmetric Si–O–Si stretching peak [$\nu_s(\text{Si–O})$] at $\sim 1100\text{ cm}^{-1}$, typical of silsesquioxane cages,^{56,57} was present in all spectra and was used as an internal reference. The consistent presence of this peak demonstrates that the structure survives processing. If the cube structure were degraded, one would observe a transformation to asymmetric broad peaks more typical of silica.^{57–59}

Table 3. Characteristic Absorptions of Various Functional Groups of Epoxy and Siloxane Composites^{44,59}

Functional group	Wavenumber (cm^{-1})	Vibration type
Si–H	~ 2200	ν_s
Si–H	800–950	δ_s
Si–C	1250	ν_s
Si–O–Si	1030–1110	ν_s
N–H	1580–1650	δ_s
N–H	3400–3500	ν_s, ν_{as} , doublets
C–N	1250–1360	ν_s
O–H	3200–3500	ν_s
C–H, aliphatic	2840–3000	ν_s, ν_{as}
C–H, aliphatic	1370–1450	δ_s
C–H, aliphatic	1150–1350	ω, τ
C–H, aromatic	3000–3100	ν_s
C–H, aromatic	675–900	out-of-plane bending
C–H, aromatic	1000–1300	in-plane bending
C=C, aromatic	1400–1500, 1580–1600	ν_s
	1250	ν_s
	810–950	ν_{as}
	750–840	ν_s , 12 μ band
C–H in 	2990–3050	ν_s

^a ν_s : symmetric vibration. ν_{as} : asymmetric vibration. δ_s : in-plane bending (scissoring). ω : out-of-plane bending (wagging). τ : out-of-plane bending (twisting).

Several network functional groups are easily observed in the spectra. Symmetric and asymmetric N–H bands appear as doublets at 3300–3500 cm^{-1} in the DDM spectrum. In addition, DDM derived N–H scissoring [$\delta_s(\text{N–H})$] at 1617 cm^{-1} and C=C aromatic ring [$\nu_s(\text{C=C})$] absorptions at $\sim 1500\text{ cm}^{-1}$ are present in all spectra except for pure OG. The intensities of these two bands decrease with increasing amounts of OG in the composite formulation because of dilution. The $\delta_s(\text{N–H})$ intensities decrease compared to those for $\nu_s(\text{C=C})$, as N–H bonds disappear and new C–N bonds form on curing, while the C=C bonds remain.

(56) Marcolli, C.; Calzaferri, G. *Appl. Organomet. Chem.* **1999**, *13*, 213.
 (57) Wallace, W. E.; Guttman, C. M.; Antonucci, J. M. *Polymer* **2000**, *41*, 2219.

(58) Chen, Y.; Iroh, J. O. *Chem. Mater.* **1999**, *11*, 1222.
 (59) Silverstein, R. M.; Webster, F. X. *Spectrometric Identification of Organic Compounds*; John Wiley & Sons: New York, 1996; p 71.

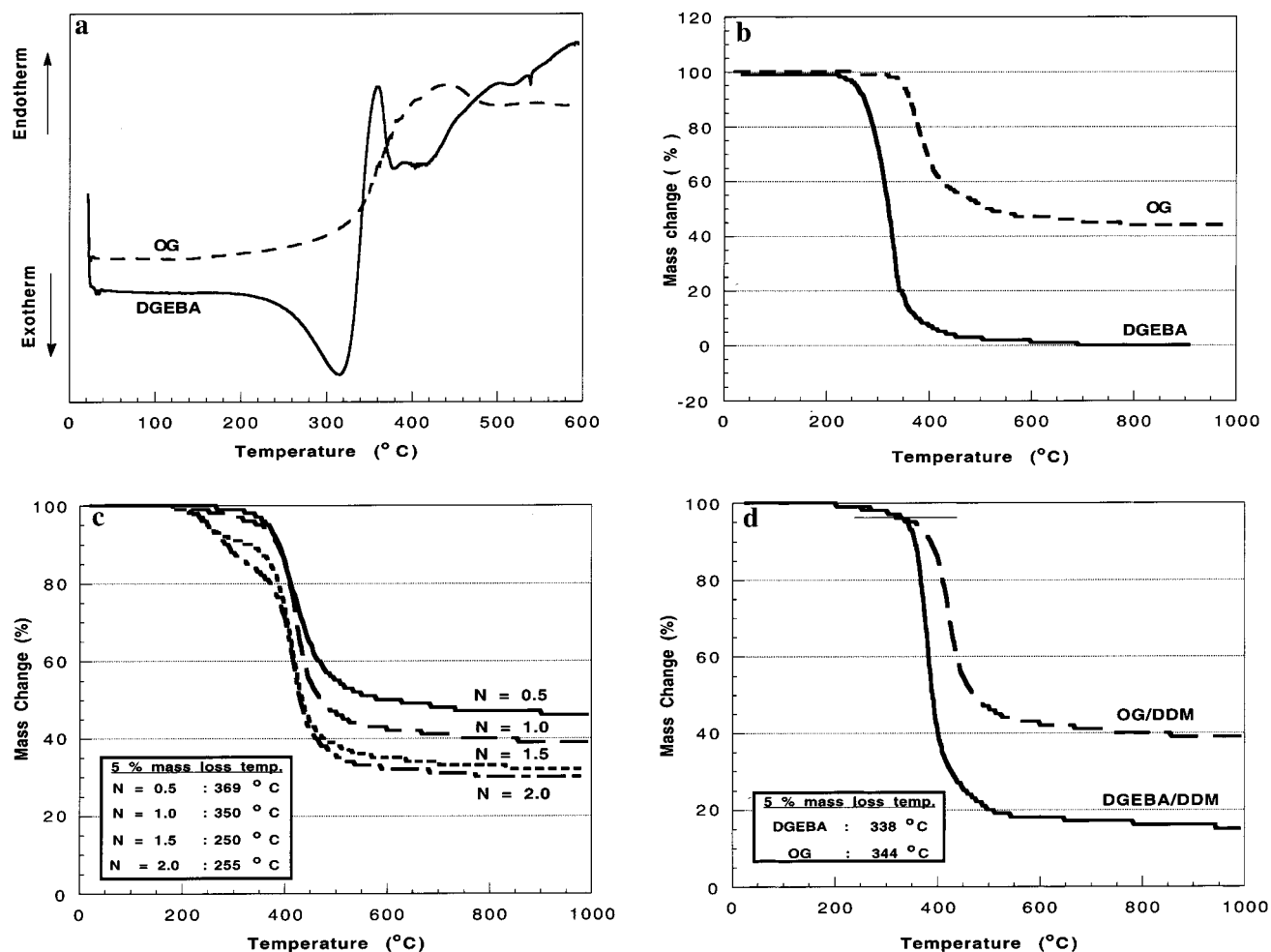


Figure 2. Thermal characterizations of various materials. All tests were performed at 5 °C/min ramp rate under N₂: (a) DSC of pure DGEBA and OG resins; (b) TGA of pure DGEBA and OG resins; (c) TGA of OG/DDM composites with various *N*'s; (d) TGA of DGEBA/DDM and OG/DDM composites at *N* = 1.0.

Weak aromatic $\nu_s(\text{C-H})$ absorptions appear at 3000–3300 cm^{-1} (DDM) in the cured structure in contrast with strong signals from pure DDM. Aliphatic $\nu_s(\text{C-H})$ bands are observed consistently at 2800–3000 cm^{-1} . Epoxy ring symmetric and asymmetric stretching^{44,59} at ~ 1250 and ~ 910 cm^{-1} , respectively, are relatively clear in pure OG but diminish and weaken in cured samples as epoxy rings are diluted by DDM in composite formulations and react on curing. Unfortunately, the $\nu_s(\text{O-H})$ bands generated from the epoxy rings on curing are not distinct in spectra of cured samples. Note that the band at 1250 cm^{-1} is an overlay of the epoxy stretch and $\nu_s(\text{Si-C})$ for the spacer groups.

Differential Scanning Calorimetry (DSC) and Thermal Gravimetric Analysis (TGA) of Reactants. Figure 2a,b compares DSC results, including the thermal stabilities of pure DGEBA and OG monomers (N₂). DGEBA decomposes at 250–350 °C under N₂ leaving only traces of char. However, DGEBA exhibits an exotherm at 250–320 °C suggesting ring opening self-polymerization. The resulting polyether network and any residual, unreacted DGEBA are likely to decompose together. In comparison, OG shows no exotherm (multiple DSC runs) even though it appears to polymerize before it decomposes at ~ 400 °C under N₂. The ceramic yield obtained in nitrogen was 44 wt %. In air, OG decomposition onset begins at ~ 230 °C, and the found ceramic yield of 48.3% is close to that expected theoretically (49.7%). The slight difference arises either from

incomplete substitution during synthesis or because of partial sublimation^{9–15} which is observed with many other octafunctional cubes. The latter possibility appears more likely given the lower than expected ceramic yield in nitrogen where sublimation is much more likely to compete with thermal degradation because of the absence of oxidative processes.

Thermal Gravimetric Analysis (TGA) of Composites. The thermal stabilities (N₂) of a series of OG/DDM composites are given in Figure 2c. In a comparison of the thermal stabilities of composites, 5% mass loss temperatures were used as standard.

In general, initial mass loss for all of the composites begins at ≈ 200 °C. However, when *N* > 1, significant mass losses occur at ≤ 350 °C, while composites at *N* ≤ 1 are relatively stable to this temperature. This contrast is clearly demonstrated by comparing 5% mass loss temperatures. They are ~ 350 °C for *N* = 0.3 and *N* = 1.0 and ~ 250 °C for *N* = 1.5 and *N* = 2.0. As we will show below, most of the curing agent up to *N* = 1 is contained within the network structure by forming at least two cross-links between the cubes. For *N* ≤ 1 , mass loss before 350 °C is insignificant indicating a trivial amount of unreacted DDM. However with excess DDM, pendant or unreacted DDM must exist and likely decomposes/fragments or volatilizes on heating. This instability becomes more pronounced with increases in DDM content. These results (and DMA/GPC data discussed below) suggest that at *N* ≤ 1 , DDM forms two to four cross-links. In these cases, unreacted OG moieties may remain, decomposing eventually at 400 °C.

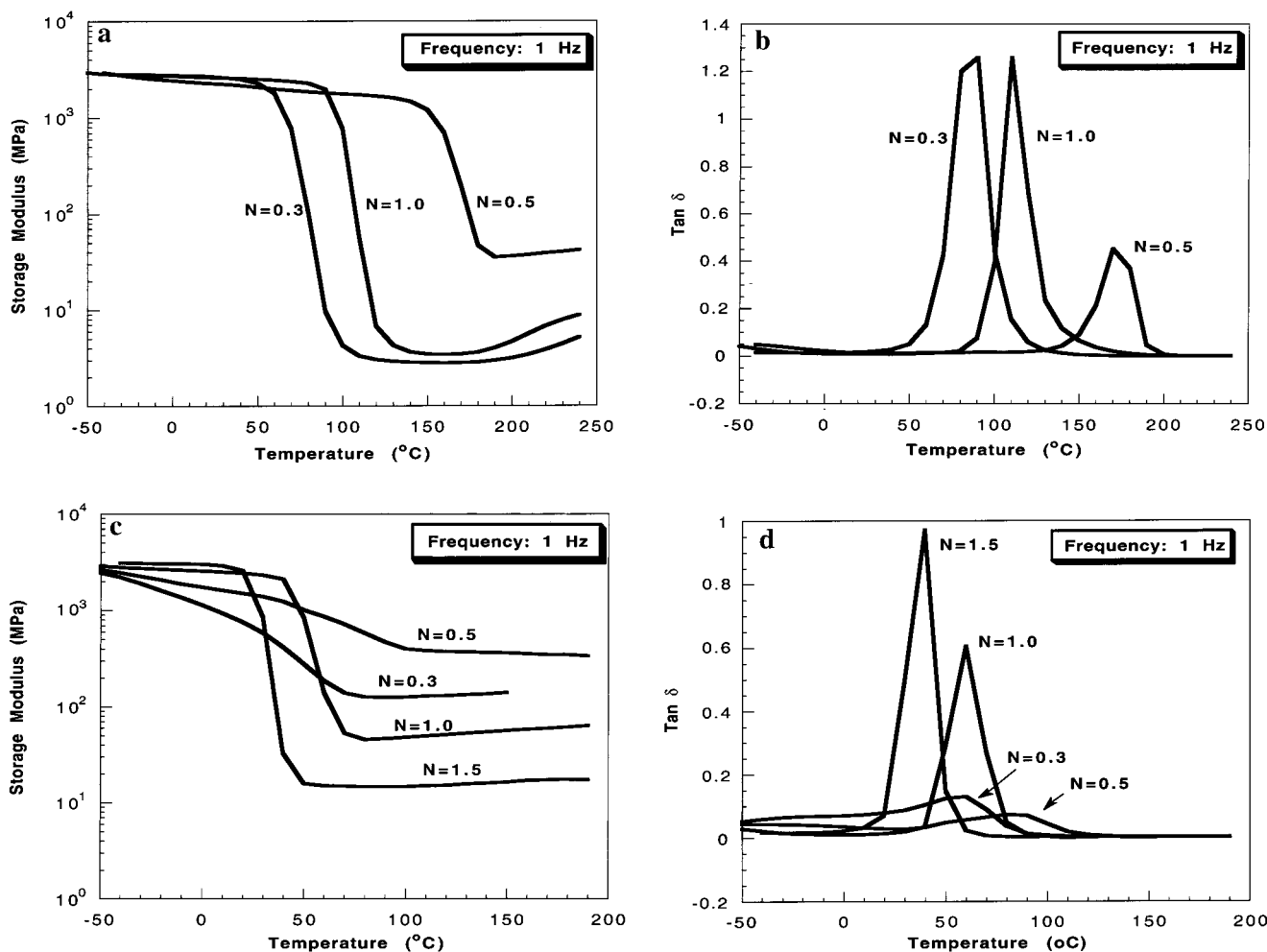


Figure 3. DMA tests of composites at various N 's: (a) storage modulus of DGEBA/DDM; (b) $\tan \delta$ of DGEBA/DDM; (c) storage modulus of OG/DDM composites; (d) $\tan \delta$ of OG/DDM composites.

Instability caused by DDM is also found in char residues. The more curing agent added (thus the subsequent lower cube loading), the lower the char, as expected. In contrast, all samples decompose significantly at the same time, i.e., lose about half of their mass, at 400–450 °C. This suggests that the organic tethers define nanocomposite instability given that the above char yields indicate that the inorganic component will likely not volatilize. The different char yields are caused by different cube loadings. A further point is that cross-linking appears to improve thermal stability given that pure OG decomposes in the 350–400 °C range under N_2 . Thus cross-linking improves thermal stabilities as much as 50 °C.

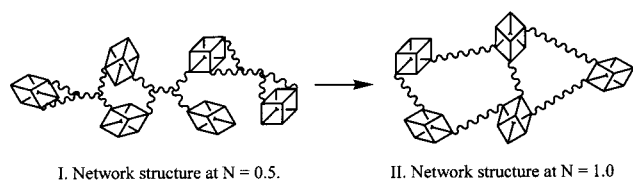
The thermal stabilities of DGEBA/DDM and OG/DDM composites at $N = 1$ where optimal mechanical properties are observed are compared in Figure 2d. Contrary to the thermal stabilities of pure DGEBA and OG, the 5% mass loss temperatures for these composites are almost identical at about 340 °C. This is not unexpected, if the organic tethers determine the thermal stability. However, the primary decomposition temperature (half mass loss point) for OG/DDM composites is higher than that of DGEBA/DDM by ~50 °C. The char residue (N_2) for OG/DDM (~40%) is also higher than DGEBA/DDM (17%) as expected because of the high silica content. In air, OG/DDM at $N = 1.0$ produces a 32.0% ceramic yield vs 35.2% (theory).

The difference in primary decomposition temperatures is important because it may be construed as an effect of creating a nanocomposite. One might argue that, in the nanocomposites, their thermal motion is restricted thereby reducing the organic

decomposition pathways accessible to the tether. It is likely that the inorganic component provides additional heat capacity thereby stabilizing the bulk material against thermal decomposition except at surfaces where initial decomposition would be expected to begin. The somewhat lower than expected char yield in air may be ascribed to some volatilization.

Dynamic Mechanical Analysis (DMA). Figure 3 shows the DMA of DGEBA and OG composites. Because we were only interested in T_{gs} (α transition) caused by main chain motion, not in secondary transitions, the lowest temperature examined was –50 °C.

Two important features can be found in comparing the storage modulus profiles of DGEBA/DDM and OG/DDM. First, the maximum rubbery state modulus is found at $N = 0.5$ for both composites. In a cross-linked structure, a rubbery state modulus relates directly to the network cross-link density. On the basis of chemistry, the maximum cross-link density is expected at $N = 0.5$ (Scheme 2), which appears in DMA as the maximum rubbery state modulus and the highest T_g . The trend for DGEBA/DDM is consistent with the literature.^{33–46} It also confirms that, in OG/DDM nanocomposites, DDM acts as a tetrafunctional reactant. The other important observation is that while DGEBA/DDM clearly shows T_{gs} for all formulations typically accompanied by a decrease in modulus of 3 orders of magnitude, OG/DDM does not exhibit an abrupt change in modulus at $N = 0.3$ or 0.5. At $N = 0.5$, its rubbery state modulus is close to 500 MPa, 1 order of magnitude larger than that of DGEBA/DDM,

Scheme 4. Illustration of the Change in Network Structure with Varying Amounts of DDM^a

^a Two, three, and four cubes can be linked to DDM at $N = 0.5$ (I). Linear tethers connecting two cubes dominate the network structure at $N = 1.0$ (II)

suggesting that the usual relaxation motion of the chains upon heating is highly hindered, likely because of the presence of cubes.

This α transition is caused by main chain motion and is usually a measure of the glass transition temperature (T_g). For example, T_g s are found to be ~ 110 and ~ 60 °C for DGEBA/DDM and OG/DDM at $N = 1.0$, respectively (Figure 3a,c). This change can more clearly be identified from the peak positions in $\tan \delta$ profiles in Figure 3b,d. While all of DGEBA/DDM and some of OG/DDM $\tan \delta$ curves exhibit clear peaks, this transition is barely noticeable for OG/DDM at $N = 0.5$. This observation suggests that the OG/DDM composite at this formulation is much more highly cross-linked, such that the main chains are bound by cross-links and their relaxation motion is hindered significantly. However for $N > 0.5$, the extra DDM allows increased motion of tethers (by decreasing cross-link density and/or increasing the number of pendant groups) and the T_g becomes more apparent and detectable by DMA.

The lack of a T_g in OG/DDM (at $N = 0.5$) can be explained as arising from a much higher cross-link density than possible in DGEBA/DDM. Because OG and DGEBA have the same glycidyl epoxide group, the cross-linking process should proceed similarly at roughly the same temperature and in the same time period, providing similar degrees of cure. However, OG is octafunctional and the core is inorganic while DGEBA is only difunctional and linear. The additional multiple inorganic cross-links in the cube provide extremely high cross-link densities in OG/DDM, and thus, any significant differences in the network mechanical properties are likely to emerge from this effect, such as in high rubbery state modulus and the lack of T_g . The inorganic cross-links, however, do not seem to affect the room-temperature modulus and toughness significantly; see below.

Although DDM behaves as a tetrafunctional compound generating two bifurcated tethers between the cubes when $N \leq 0.5$, the formation of linear tethers (completely discontinuous nanocomposites) will be favored for $N \geq 0.5$ if curing of the first N–H is faster and favored over the second one. When DGEBA is cured with a series of aliphatic amines such as *n*-butylamine or 1,2-ethanediamine, the first hydrogen reacts twice as fast as the second hydrogen does.⁴⁷ Aromatic amines cure more slowly than aliphatic amines.⁴⁷ In slow curing, the higher reaction rate has a more pronounced effect. This reactivity difference can be related to steric factors.

The steric hindrance will be even greater for bulky OG, and curing using aromatic DDM should strongly favor reaction of the first hydrogen. Therefore, linear tethers instead of bifurcated ones should dominate the structure at $N \approx 1$. This argument is supported by data presented below. Schematic representations of OG/DDM nanocomposite network structures with different amine contents are suggested in Scheme 4.

An important point to note is that the T_g for OG/DDM at $N = 1$ is ≈ 60 °C which is lower than that found for the DGEBA/DDM

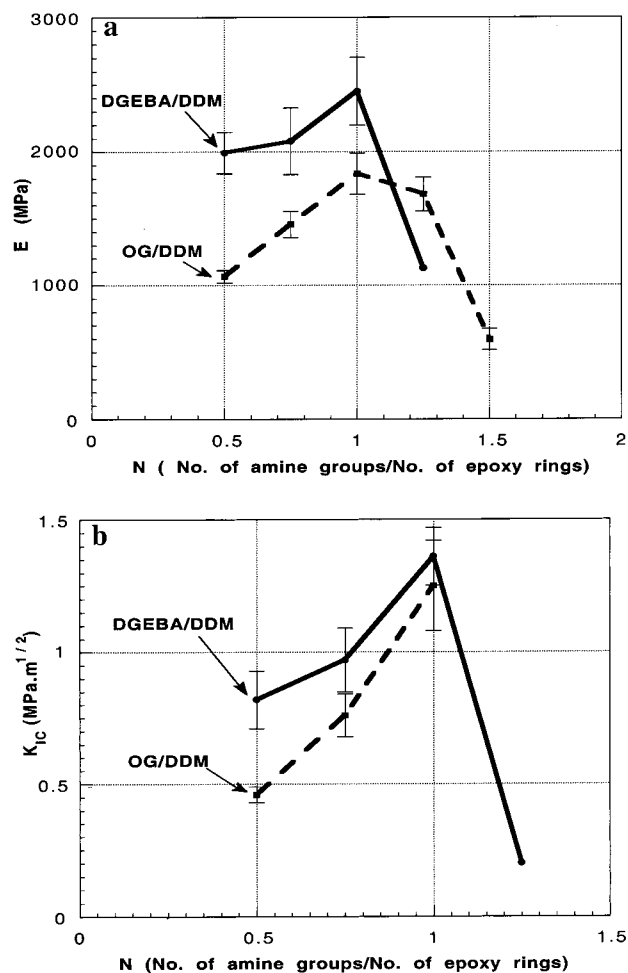


Figure 4. Room-temperature mechanical properties at various N 's: (a) tensile modulus (E) of DGEBA/DDM and OG/DDM composites; (b) fracture toughness (K_{1c}) of DGEBA/DDM and OG/DDM composites.

DDM material ($N = 1$, $T_g \approx 110$ °C). This contrasts with our argument about the much higher cross-link density expected with OG. It may reflect the fact that the N–H and OH groups in the DGEBA/DDM/ $N = 1$ composite are free to hydrogen bond⁶⁰ with each other but are constrained from close approach in the rigid tethers of OG/DDM/ $N = 1$. Evidence for H-bonds playing a major role in the T_g can be found in the substantial lowering of T_g in amine-cured epoxies on absorption of water.⁶⁰ It will be interesting to see if OG/DDM/ $N = 1$ is sensitive to moisture.

Cross-linking between the epoxy ring and OH groups generated by epoxy ring opening is not likely because this reaction is relatively slow and usually takes place only after all amine functionality is consumed.⁴⁷ In our studies, amine contents are equal to or greater than epoxides for all samples except for $N = 0.3$. Besides, once the rings open due to curing, the steric hindrance and the increased viscosity in the neighborhood will limit further intermolecular reactions.

Room-Temperature Mechanical Properties. The room-temperature tensile moduli of DGEBA/DDM and OG/DDM composites are compared in Figure 4a as a function of N . Each data point represents an average of at least five samples. All testing was done below the T_g s of all the composites made.

Interestingly, both DGEBA/DDM and OG/DDM show the same modulus profile with respect to amine content. They

(60) Kaelble, D. H. In *Epoxy Resins, Chemistry and Technology*; May, C. A., Ed.; Marcel Dekker: New York, 1988; p 603 and references therein.

Table 4. Mechanical Properties of Selected DGEBA Resins Cured with Various Amines

DGEBA	amine ^a	N ^b	T _g (°C)	E (GPa)	K _{1C} (MPa ^m ^{1/2})	ref
DER 331	DDM	0.5	164	2.6 (compression)	0.85	33
Epikate828	DDM	0.5			1.12	34
Epon 828	DDM	0.5	175	1.07		35
Epon828	PACM	0.5	165	2.5		36–38
Epon828	DDS	0.5	200		1–2	39
Epon828	piperidine		90–100 ⁴³	2.941	1–2 ⁴⁰	40, 41
DER332	3DCM	0.5	183	2.65	0.78	42
Epon825	EDA	0.5		2.7	0.73	43
DER331	DETA	0.5		1.7		44
Epon828	PDA	0.5	160	3.7	0.6–1	45
DER332	Jeff	0.5	93	2.3		46

^a 4,4'-Diaminodiphenylmethane (DDM), bis(*p*-aminocyclohexyl)methane (PACM), diaminodiphenyl sulfone (DDS), 4,4'-diamino-3,3'-dimethylidicyclohexylmethane (3DCM), ethylenediamine (EDA), diethylenetriamine (DETA), and 1,2-phenylenediamine (PDA). ^b *N* is defined as the molar ratio of amine groups per epoxy ring. This variable is consistently used in this study. See the Experimental Section.

exhibit maxima of 2.4 ± 0.25 and 1.8 ± 0.15 Gpa, respectively, at $N \approx 1$. However, the decrease in tensile modulus at $N > 1$ is more drastic for DGEBA/DDM than for OG/DDM. At the same composition at $N > 1.0$, DGEBA/DDM becomes very brittle, as revealed by toughness measurements, with moduli well below those of OG/DDM. In contrast, OG/DDM maintains its maximum modulus up to $N \approx 1.25$. Above this point, the modulus drops as N increases due to lower T_g s.

While DGEBA/DDM becomes brittle with excess DDM ($N > 1.0$), OG/DDM becomes rubbery. (“Excess” is used for $N > 1$ unless stated otherwise. In the general epoxy literature, the term “excess” typically corresponds to $N > 0.5$.) At $N \approx 2$, the modulus of OG/DDM cannot be measured because of the rubberlike behavior and is not included in Figure 4a. This behavior also reflects in the fracture toughness data.

The fracture toughness of DGEBA/DDM and OG/DDM were tested in tension. The critical stress intensity factors (K_{1C}) are compared in Figure 4b. As in the tensile tests, both DGEBA/DDM and OG/DDM share the same profile and maxima are reached at $N \approx 1$. The K_{1C} 's for both materials are the same within the error. When DGEBA is cured with excess DDM, however, the material changes from a ductile to a brittle material and fracture toughness drops significantly. In contrast, OG/DDM composites become rubbery with excess DDM due to the lowered T_g , and it is impossible to introduce a natural crack into these samples. Consequently, no data points for $N \geq 1$ are included in Figure 4b.

Table 4 lists the mechanical properties of some DGEBA resins prepared using various curing agents. In these studies, the highest cross-link densities are obtained at stoichiometries where two epoxy ring equivalents are mixed with one amine group equivalent (the ratio of epoxy ring to amine *hydrogen* was 1:1). At this highest cross-link density, the glass transition temperatures are maximized.^{36–39}

Although different trends have been reported for the room-temperature mechanical properties^{33–46} of cured epoxy resins implying no direct relationship between network structure and room-temperature properties, most materials exhibit a global *minimum* for the glassy state modulus for stoichiometries of $N = 0.5$ (N is defined as the molar ratio of NH_2 groups per epoxy ring). Fracture toughness also increases as the amine content increases above $N = 0.5$. In contrast, for our materials, the greatest rubbery state moduli at temperatures above the glass transition temperature (T_g) are observed at $N = 0.5$.

In contrast to many literature values, the maximum modulus and the fracture toughness values for both composites prepared here are obtained at $N \approx 1$. Surprisingly, this formulation is not where the highest cross-linked density is obtained. (DMA studies show the maximum cross-link density at $N = 0.5$ for

both composites.) This implies that some degree of chain flexibility provides optimal mechanical properties.

The highest cross-link density which is obtained at $N = 0.5$ implies that DDM is tetrafunctional on curing. Consequently, the dominating organic tether structure at $N = 0.5$ is expected to be the one in which DDM connects four cubes (Schemes 2 and 4). Ideally, complete reaction of epoxides and amines at this formulation will lead to cubes that only have four-armed organic tethers, although this is statistically not possible (see below).

Two restrictions hinder the formation of a perfect network structure. First, before all the epoxy rings and amines can react and cross-link, the viscosity during curing will increase to the point where it becomes impossible for unreacted functional groups to find each other. These unreacted organic tethers will remain as pendant groups. The other restriction is that the two hydrogens in the primary amine group are not necessarily equally reactive. Reaction of the first may be favored over the second one, and as a result, another uniform and densely cross-linked structure can be obtained at $N = 1$. Linear tethers connecting two cubes may be the dominating structures (Scheme 4, II). Certainly both restrictions apply to the current system and the network structure of the OG composites is likely not perfect. Real networks should, on a statistical basis, contain all types of organic tethers. A more in-depth discussion regarding network structures follows.

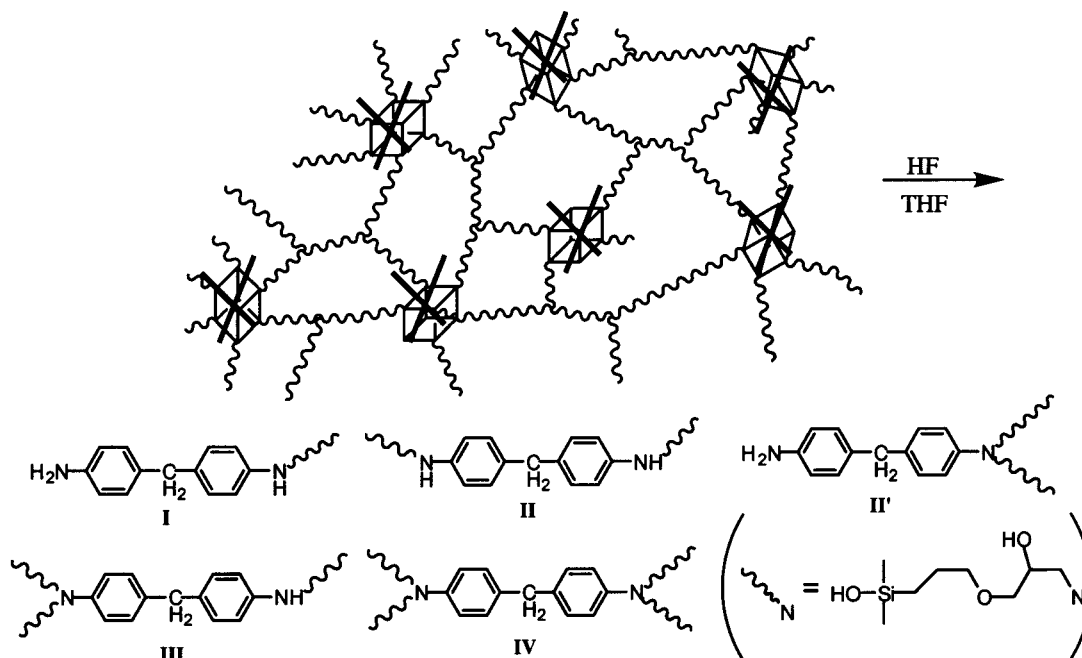
Model Curing Studies. Because of the cross-linking, it would be impossible to investigate the curing behavior or to characterize the network using conventional techniques such as ¹H NMR or GPC that require dissolution of the material. Besides, direct characterization of the cross-linked structure would generate complicated data due to the complexity of the cross-linked network. Preliminary solid-state NMR studies gave inconclusive results.⁶¹

Thus, model studies on the reactive components alone were undertaken. Allyl glycidyl ether/DDM mixtures were reacted to probe the functionality of DDM involved in network formation. Because the oligomeric organic products are not bound to the cubic cores, study by solution NMR becomes possible. Also the low viscosity of the mixture will not limit reactions between epoxides and amines.

In these studies, all the epoxide rings react with DDM completely at $N \geq 0.5$. This result suggests that DDM will be completely tetrafunctional under ideal curing conditions where curing is not limited by high viscosity or steric hindrance. Therefore, in curing OG/DDM, four-armed tethers are likely

(61) Babonneau, F.; Choi, J.; Laine, R. M. Unpublished work.

Scheme 5. Possible Organic Tether Structures



avored at $N \leq 0.5$. At $N = 1$, almost complete reaction is also observed with the two-arm tethers form predominating (see below).

Unfortunately, exact structures at $N > 0.5$ cannot be determined in this test only because there is a statistical probability of producing four-, three-, two-, and one-armed tethers in these model systems. However, they can be estimated using GPC as discussed below.

Tether Structure Studies by GPC. After the above studies were complete, we realized that, if Si–O bonds were broken by HF, the resulting organic tethers would be soluble in conventional solvents.⁵⁵ Then, by measurement of molecular weights and distributions using GPC, overall network structures could be understood. This approach provides rare insight into network structures not available in wholly organic materials. Because products in the above model curing studies are ideal structures without inorganic components, their GPC chromatograms can be used as standards to identify the peaks in GPC chromatograms of real tethers. Theoretically, five different tether structures can be produced during curing (Scheme 5).

Figure 5 compares the molecular weights and distributions of model tethers and real ones. THF-extracted oligomeric organic tethers were directly analyzed by GPC after filtering (see Experimental Section). In model compounds (Figure 5a), pure DDM appears as a narrow peak at 35.5 min. A single peak is also observed for $N = 0.3$ at 31.5 min suggesting that the structure is entirely IV. Excess amounts of allyl glycidyl ether at $N = 0.3$ guarantee the formation of four-armed tethers. However, at $N = 0.5$, a shoulder at 32 min appears beside the main peak. This shoulder is thought to be a three-armed tether III. At $N = 1.0$ and 1.5, the peak for the four-armed tether (31.5 min) disappears completely and the peak at 32.5 min becomes dominant along with the one at 33.3 min. These two peaks are thought to be tethers II and I, respectively. Unreacted pure DDM is also found at 35.5 min. These results suggest that the tether IV dominates at $N \leq 0.5$, but tethers III, II, and I form the basis for the network structure at $N \approx 1.0$ with II providing the primary cross-links as type I components do not contribute to cross-linking. Unfortunately, II and II' cannot be differentiated in the GPC chromatogram. This study assumes

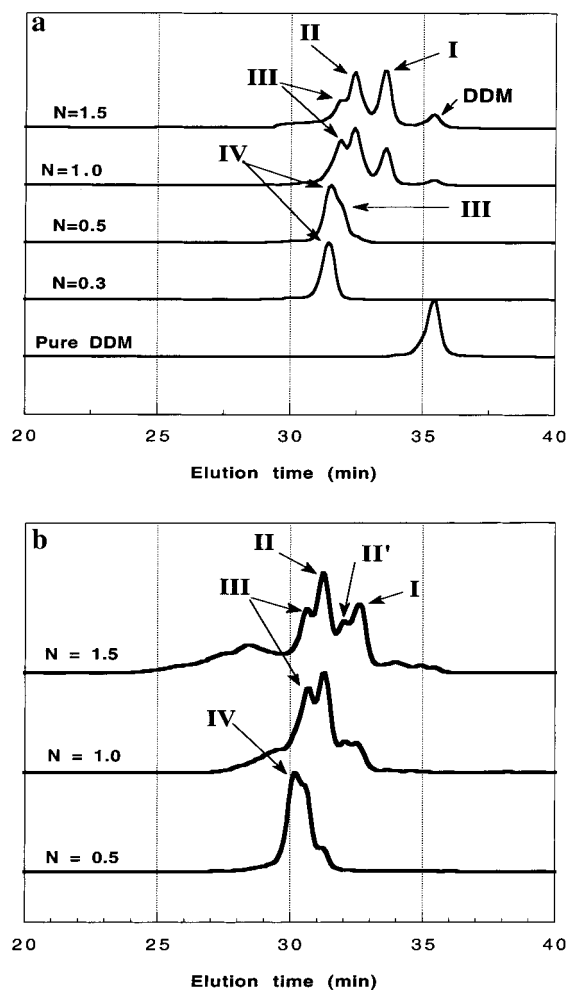


Figure 5. GPC chromatograms of model and recovered organic tethers: (I) one-armed tether; (II) two-armed tether; (II') two-armed tether; (III) three-armed tether; (IV) four-armed tether; (a) allyl/DDM model tethers without inorganic components; (b) OG/DDM tethers prepared after removing inorganic components by HF.

that the hydrodynamic volume of **II'** is similar to that of **II** or of **I** such that it cannot be observed separately.

Tethers recovered by core dissolution offer more complicated GC chromatograms than the model compounds (Figure 5b). First, all the peaks are shifted to lower elution times. This is because the tethers contain dimethylsilyl groups at each chain end. These groups increase the tether size, and thus, they appear in higher molecular weight regions. Second, the shoulder profiles are more complex. At $N = 0.5$, two shoulders are observed at 30.5 and 31.0 min besides the four-armed tether peak at 30.0 min. They are thought to be the three-armed tether **III** and two-armed **II**, respectively. These two peaks become dominant at $N = 1.0$ and $N = 1.5$, and the one at 30.0 min completely disappears as in the model curing study. However, another two peaks are observed between 32.0 and 33.0 min, which are equivalent to the one-armed tether peak in model structures. This is probably because dimethylsilyl groups attached at the chain ends make tethers **II** and **II'** distinguishable in size and thus **II'** can be detected separately. That is, **II'** is expected to appear before **I** and after **II**. Only trace amounts of unreacted DDM are seen suggesting nearly complete curing. The small peaks at 28.0 min region, particularly at $N = 1.5$, seem to originate from the incomplete digestion of the sample.

These results support our initial hypothesis that linear two-armed tethers will be the dominating structure at $N = 1.0$ due to disparities in the N–H reaction rates and steric hindrance during curing. Network structures at $N = 0.5$ also turn out to be very uniform, consisting of four-armed tethers as expected.

Conclusions

These findings suggest several important conclusions about the OG/DDM system. First, they suggest that we can make highly homogeneous nanocomposites with good-to-excellent control of the nanoarchitecture. Hence we can produce nanocomposites with essentially completely defined inorganic and organic phases. Furthermore, these results suggest that we can

tailor the nanoarchitecture fairly easily. For example we can make nanocomposites with very uniform two-armed tethers at $N = 1.0$, if (1) steric hindrance is utilized and if (2) bulky epoxides or (3) amines are part of the resin system. Then, only linear two-armed tethers will form in preference to 3- or 4-armed ones. *These materials are expected to consist of completely discontinuous organic/inorganic nanoarchitectures.*

Additional findings are that by tailoring the nanoarchitecture, we can prepare nanocomposites that exhibit quite different mechanical properties, e.g., in OG/DDM at $N = 0.5$ vs $N = 1$. Furthermore, the above results provide some support for changing the properties (e.g., thermal stability) through the use of nanosized inorganic particulates.

Finally, it should be noted that the moduli and fracture toughness of the nanocomposites are no higher than those of the organic resins. The thermal stabilities are no different from the organic resins. There are however differences in the T_g s and the mechanical properties at different compositions. Some of this can be explained by higher cross-link densities resulting from the presence of the rigid cubic core. The implication is that the organic tethers mediate the mechanical properties and thermal stabilities.

What we have not done here is to show that small changes in organic nanoarchitecture can have significant changes in mechanical properties. Nor have we shown that modeling can be used to demonstrate that the observed effects can be explained by the tether architecture. In related work, with ethylcyclohexene epoxide cubes, we are able to demonstrate all of these points.^{16,54}

Acknowledgment. We would like to thank the FAA for their initial support of this work through Grant No. 95-G-026. This work was also supported in part by the U.S. Air Force through a contract with Phillips Laboratories, Edwards AFB. J.H. and A.F.Y. thank AFOSR for partial support of this work.

JA010720L